Phase Field Simulation of Dendritic Microstructure in Additively Manufactured Titanium Alloy

Jing Zhang*, Linmin Wu, Yi Zhang, Lingbin Meng

Department of Mechanical Engineering, Indiana University-Purdue University Indianapolis, Indianapolis, IN 46202, USA

*Email: jz29@iupui.edu; Phone: 317-278-7186; Fax:317-274-9744

Abstract

Additive manufacturing (AM) processes for metals, such as selective laser sintering and electron beam melting, involve rapid solidification process. The microstructure of the fabricated material and its properties strongly depend on the solidification. Therefore, in order to control and optimize the AM process, it is important to understand the microstructure evolution. In this work, using Ti-6Al-4V as a model system, the phase field method is applied to simulate the microstructure evolution in additively manufactured metals. Frist, the fundamental governing equations are presented. Then the effects of various processing related parameters, including local temperature gradient, scan speed and cooling rate, on dendrites morphology and growth velocity are studied. The simulated results show that the dendritic arms grow along the direction of the heat flow. Higher temperature gradient, scan speed and cooling rate will result in small dendritic arm spacing and higher growth velocity. The simulated dendritic morphology and arm spacings are in good agreement with experimental data and theoretical predictions.

Keywords: phase field; metals; temperature gradient; scan speed; additive manufacturing

---

This is the author's manuscript of the article published in final edited form as:

Zhang, J., Wu, L., Zhang, Y., & Meng, L. (2019). Phase field simulation of dendritic microstructure in additively manufactured titanium alloy. Metal Powder Report, 74(1), 20–24. https://doi.org/10.1016/j.mprp.2018.11.001

1. Introduction

During additive manufacturing process, due to the cooling, solidification and phase transformation occur in the melt pool [1, 2]. This will significantly affect the material properties of the build materials, since solidification controls the morphology of the microstructure. Thus, it is essential to understand the solidification behavior during the fabrication. Titanium based alloys, especially Ti-6Al-4V, are widely used in aerospace, biomedical and automotive industries due to their excellent mechanical strength and creep resistance at high temperatures [3-5]. Recently, many studies were carried out to investigate the microstructures and material properties of laser deposited Ti-6Al-4V by experiment [6-10]. However, due to the short time scale of the solidification and the small length scale of the melting pool, it is very difficult to study the microstructure evolution during the fabrication process by experiment. Hence, numerical simulations aiming to reveal microstructure evolution during the solidification process are warranted.

Phase field method is a promising technique to describe the microstructure evolution [11-13]. It has been used to simulate the dendrites growth in undercooled pure materials [14, 15], and has been extended to describe the dendrites morphology in binary alloys [16-19]. For Ti-6Al-4V, only few studies have been carried out by phase field method. Gong and Chou [20] applied phase field method to investigate the columnar grain growth of Ti-6Al-4V during solidification and compared grain sizes with experimental results. Sahoo and Chou [21] studied the dendritic arm spacing with different processing parameters in electron beam additive manufactured Ti-6Al-4V. In this study, the phase field method will be employed to simulate the phase transformation from liquid phase to solid prior β phase of Ti-6Al-4V during rapid solidification. The influence of the local temperature gradient, scan speed and cooling rate will be investigated. Ghosh *et al.* studied

the primary spacing and microsegregation of cellular dendrites in laser deposited Ni–Nb alloys[22]. A phase-field model is used to simulate solidification microstructures at different locations within a solidified molten pool. Although the phase-field model has an anti-trapping solute flux term meant to maintain local interface equilibrium, it is found that during simulations it was insufficient at maintaining equilibrium. This is due to the fact that the additive manufacturing solidification conditions fall well outside the allowed limits of this flux term[22].

This work is based on our previous research [23], with revised contents. First, the fundamental governing equations are presented. Then the effects of various processing parameters, including local temperature gradient, scan speed and cooling rate, on dendrites morphology and growth velocity are studied.

2. Phase field model description

To simulate the microstructure evolution of Ti-6Al-4V during additive manufacturing process, phase field method is employed. In this study, Ti-6Al-4V is assumed to be a pseudo-binary alloy, since it is shown that the pseudo-binary approach can be a successful approximation for the multi-component approach when simulating the solidification of Ti-base alloy such as Ti-6Al-4V [24, 25].

The phase field simulations were carried out to simulate the phase transformation from liquid phase to solid prior β phase. The model consists of two coupled equations, with one describing the evolution of phase order parameter φ, and the other governs the mass transport of the composition c during the solidification of a binary alloy. The dimensionless form of governing equations is given by,

$$a(\theta)^2\frac{\partial\varphi}{\partial t}=\nabla\cdot\left[a(\theta)^2\nabla\varphi\right]-\frac{\partial}{\partial x}\left[a(\theta)\frac{\partial a(\theta)}{\partial\theta}\frac{\partial\varphi}{\partial y}\right]+\frac{\partial}{\partial y}\left[a(\theta)\frac{\partial a(\theta)}{\partial\theta}\frac{\partial\varphi}{\partial x}\right]$$
$$+\varphi-\varphi^3-\lambda\left(1-\varphi^2\right)^2\left[U+\frac{T-T_0}{m_l c_0\left(1-k\right)/k}\right] \tag{1}$$

$$\frac{\partial c}{\partial t}=\nabla\cdot\left[D\frac{1-\varphi}{1+k-\left(1-k\right)\varphi}\nabla u\right]+\nabla\cdot j_{at} \tag{2}$$

where φ is phase order parameter with $\varphi=-1$ representing solid phase and $\varphi=1$ meaning liquid phase. $a(\theta)=1+\varepsilon\cos(4\theta)$ represents the four-fold surface energy anisotropy at the solid-liquid interface with the strength of anisotropy ε and the angle between the interface normal and the x direction $\theta=\arctan\left(\partial_y\varphi/\partial_x\varphi\right)$. $k=c_s/c_l$ is partition coefficient, where c_s and c_l are equilibrium compositions on solid and liquid side of the interface, respectively. m_l is liquidus slope and c_0 is alloy concentration far from the solidification front. U is the dimensionless supersaturation, which is defined as, $U=\left(e^u-1\right)/\left(1-k\right)$, where u is a dimensionless chemical potential given by,

$$u=\ln\left(\frac{2ck/c_0}{1+k-\left(1-k\right)\varphi}\right) \tag{3}$$

The frozen temperature approximation was applied to the system, which is described by $T=T_0+G\left(y-Vt\right)$. G and V are temperature gradient and constant pulling speed along y direction, respectively. T_0 is the reference temperature.

In equation (2), $D = D_l\left(1-\varphi\right)/2 + D_s\left(1+\varphi\right)/2$ is diffusion coefficient of the system, where D_l and D_s are diffusion coefficient in liquid and solid phase, respectively. The anti-trapping current j_{at} was introduced to the diffusion equation to suppress the solute-trapping effects at the solid-liquid interface [18], and is given by,

$$j_{at} = \frac{1}{2\sqrt{2}} U \frac{\partial \varphi}{\partial t} \hat{n} \tag{4}$$

where $\hat{n} = -\nabla\varphi / |\nabla\varphi|$ is the unit vector normal to the solid-liquid interface.

There are three characteristic parameters in the phase field model, the characteristic length W, the characteristic time τ and the coupling constant λ. Based on thin interface analysis, two equations are given to describe the relationship of these three parameters,

$$\lambda = \frac{a_1 W}{d} \tag{5}$$

$$\tau = \frac{a_2 \lambda W^2}{D_l} \tag{6}$$

where d is the chemical capillary length. $a_1 = 0.8839$ and $a_2 = 0.6267$ are constant, which is given in [18].

To solve the phase field equation (1) and the mass transport equation (2), a finite volume method was used with explicit time marching. No flux boundary conditions were applied on all boundaries.

3. Results and discussion

The simulated microstructure evolution of Ti-6Al-V during solidification is shown in Fig. 1. Three features can be observed from the structures. First, the microstructure shows columnar structures. With the increase of solidification time, the initial random nuclei become unstable and start to grow. Finally, parallel dendritic arms are formed. The growth of the dendritic arms is along the direction of the heat flow, which is in y-direction in this case. Second, droplets are formed inside dendrites during the solidification. These droplets have high solute concentration. Similar results are found in the rapid solidification process of binary alloys [26, 27]. Third, there is significant micro-segregation phenomenon. It is found that solute enriches in the liquid near the dendritic tips and between dendritic arms. As the dendritic arms grow, the liquid concentration increases near the tip regions and decreases rapidly to the alloy concentration far away from the solidification front c_0.

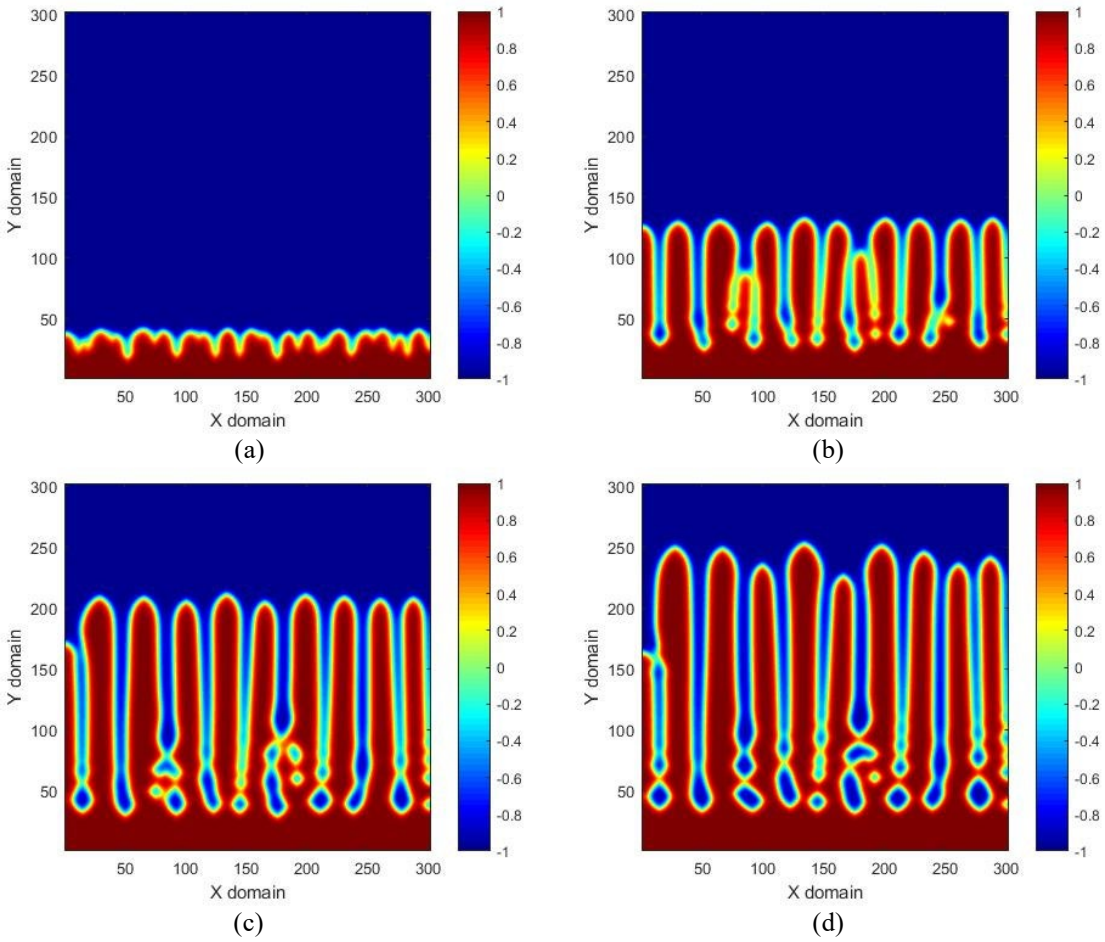

Fig. 1: Simulated columar structure at different times with $G = 2800$ K/mm and $V = 400$ mm/s. (a) 0.02 ms, (b) 0.1 ms, (c) 0.2 ms, (d) 0.3 ms.

In Fig. 2, the SEM image of electron beam additive manufactured Ti-6Al-4V sample is shown. It can be seen from the microstructure that columnar dendritic structures are formed, which is columnar prior β grains. The phase field simulations were carried out to simulate the phase transformation from liquid phase to solid prior β phase. The simulated phase and solute concentration profiles are comparable with the experimental observations.

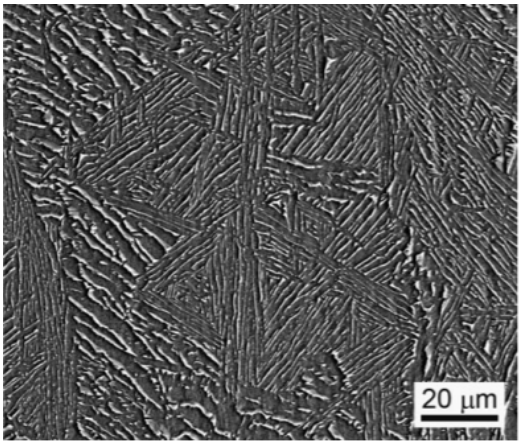

Fig. 2: SEM image of electron beam additive manufactured Ti-6Al-4V sample [28].

One important parameter used to quantify the microstructure after solidification is Primary Dendritic Arm Spacing (PDAS). Broderick *et al*. [29] investigated the effects of cooling conditions on the microstrucutre of rapidly solidified Ti-6Al-4V experimentally. The correlation between cooling rate $\dot{T}$ and PDAS is given by,

$$PDAS = A(GV)^n = A\dot{T}^n \tag{7}$$

where A and n are constants. After fitting to the experimental data, A and n are obtained as 3.1×10^6 μm $(K/s)^{1.05}$ and -1.05. In order to compare the simulation results with the experimental values, phase field simulations with constant scan speed 400 mm/s and different temperture gradient varying from 2000 K/mm to 2800 K/mm were carried out. The comparison is shown in Fig. 3. In overall, the simulated PDAS is in agreement with the experimental fitted values. It can be seen that PDAS reduces with the increasing cooling rate, implying that higher cooling rate will results in a finer columnar structure during solidification.

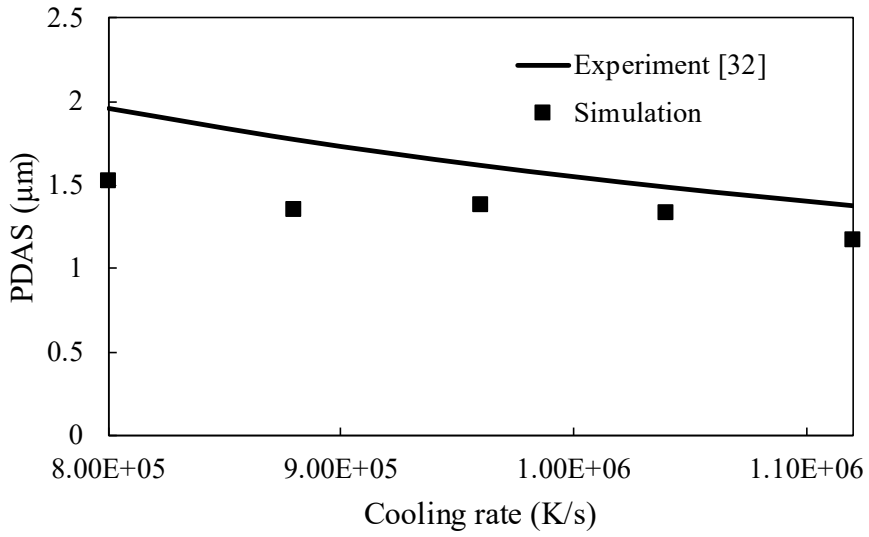

Fig. 3: Comparison of simulated PDAS values with experimental fitted results.

To study the effect of temperature gradient on microstructure, simulations with a fixed scanning speed 400 mm/s and different temperature gradient were performed. It can be seen that with the increase of the temperature gradient, the columnar structure become denser, indicating smaller PDAS. Besides, the growth velocity of the dendrites is higher when temperature gradient is larger. This result is consistent with the previous experimental data, as elavated temperature gradient means higher cooling rate. The simulated PDAS is also compared with analytical models. Hunt [30] proposed a theoretial model to predict PDAS by considering the geometry of dendrite tip. The model is given by,

$$PDAS = 2.83\left(k\Gamma\Delta T_0 D_l\right)^{0.25} G^{-0.5} V^{-0.25} \tag{8}$$

where Γ is Gibbs-Thompson coefficient and ΔT_0 is equilibrium freezing range. Kurz and Fisher [31] improved the model by considering the entire geometry, including dendrite tip and trunk. The Kurz and Fisher model is expressed by,

$$PDAS = 4.3\left(k\Gamma\Delta T_0 D_l\right)^{0.25} G^{-0.5} V^{-0.25} \tag{9}$$

The comparison is shown in Fig.4. For simulated PDAS, with the increase of temperature gradient from 2000 K/mm to 3000 K/mm, the PDAS decreases from 1.52 μm to 1.15 μm. It can be obtained that the simulated PDAS lies between the Hunt's and Kurz's results. In general, the simulated PDAS has the same trend as Hunt's and Kurz's models. The differences of the simulated results and theoretical predictions may be caused by the following reasons. First, the theoretical models were developed based on three-dimensional cases, while the phase field simulations were carried out in two dimension. Second, both models assumes the initial conditions as simple geometry, meanwhile small random pertubations were used as initial conditions in this study.

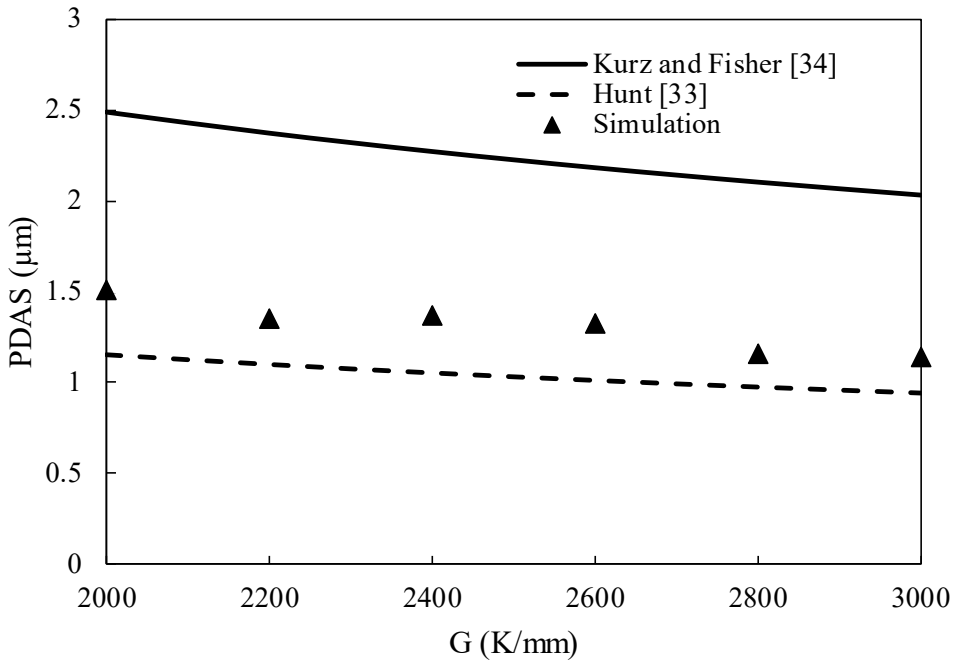

Fig. 4: Comparison of simulated PDAS with theoretical predictions. The scan speed is fixed at 400 mm/s.

The effect of scan speed on Ti-6Al-4V was studied by fixing the temperature gradient at 2000 K/mm and varing the scan speed from 200 mm/s to 800 mm/s. The comparision of the simulated PDAS with the theoretial predictions is plotted in Fig.5. For simulation results, as the increase of scan speed from 200 mm/s to 800 mm/s, the PDAS decreases from 1.58 μm to 1.36 μm, which is comparable with analytical model results.

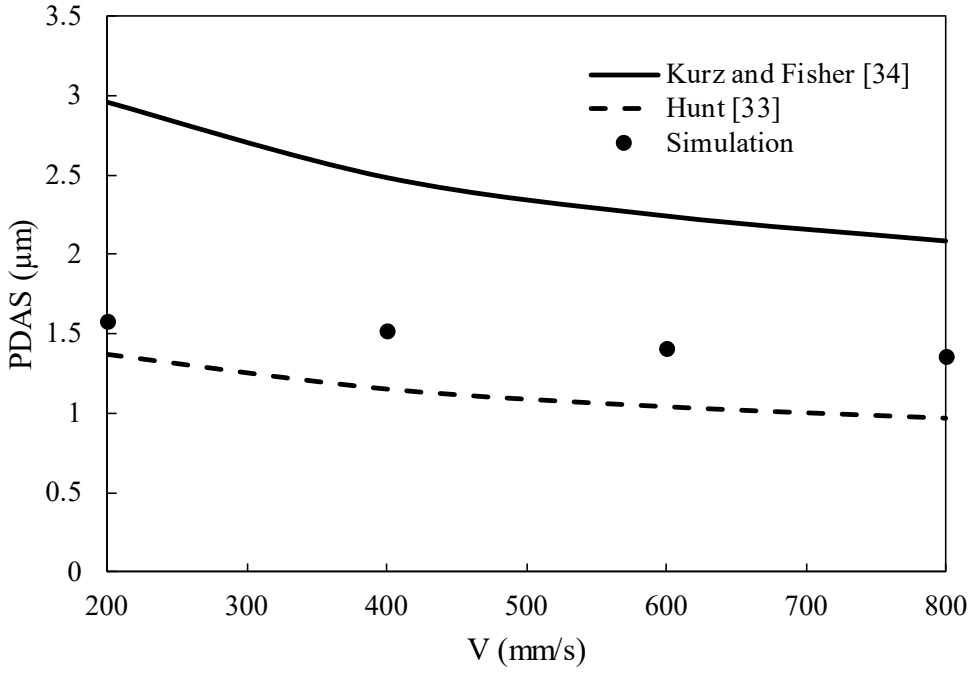

Fig. 5: Comparison of simulated PDAS with theoretical predictions. The temperature gradient is fixed at 2000 K/mm.

3. Conclusions

The microstructure evolution of additively manufactured Ti-6Al-4V during rapid solidification has been investigated using phase field method. The conclusions are summarized as follows:

(1) The phase field method can simulate the phase transformation from liquid phase to solid phase of Ti-6Al-4V during solidification. The morphology shows a columnar structure.

(2) The growth of the dendritic arms is along the direction of the heat flow. Droplets are found formed inside dendrites. Solute enriches in the liquid near the dendritic tips and between dendritic arms.

(3) Temperature gradient, scan speed and cooling rate have significant influence on dendrites morphology and growth velocity. Higher temperature gradient, scan speed and cooling rate will result in small dendritic arm spacing and higher growth velocity. The simulated results are in good agreement with experimental data and theoretical predictions.

Acknowledgment

We acknowledge the financial support provided by the Walmart Foundation (project title: Optimal Plastic Injection Molding Tooling Design and Production through Advanced Additive Manufacturing), and Praxair's TruForm AMbition Grant awarded to JZ.

References

[1] L. E. Murr, S. M. Gaytan, D. A. Ramirez, E. Martinez, J. Hernandez, K. N. Amato*, et al.*, "Metal Fabrication by Additive Manufacturing Using Laser and Electron Beam Melting Technologies," *Journal of Materials Science & Technology,* vol. 28, pp. 1-14, 2012/01/01 2012.

[2] H. L. Wei, J. Mazumder, and T. DebRoy, "Evolution of Solidification Texture during Additive Manufacturing," *Scientific Reports,* vol. 5, p. 16446, 2015.

[3] S. Zherebtsov, G. Salishchev, R. Galeyev, and K. Maekawa, "Mechanical Properties of Ti-6Al-4V Titanium Alloy with Submicrocrystalline Structure Produced by Severe Plastic Deformation," *Materials Transactions,* vol. 46, pp. 2020-2025, 2005.

[4] C. Qiu, N. J. E. Adkins, and M. M. Attallah, "Microstructure and tensile properties of selectively laser-melted and of HIPed laser-melted Ti–6Al–4V," *Materials Science and Engineering: A,* vol. 578, pp. 230-239, 8/20/ 2013.

[5] T. Vilaro, C. Colin, and J. D. Bartout, "As-Fabricated and Heat-Treated Microstructures of the Ti-6Al-4V Alloy Processed by Selective Laser Melting," *Metallurgical and Materials Transactions A,* vol. 42, pp. 3190-3199, 2011// 2011.

[6] H. Galarraga, D. A. Lados, R. R. Dehoff, M. M. Kirka, and P. Nandwana, "Effects of The Microstructure and Porosity on Properties of Ti-6Al-4V Alloy Fabricated by Electron Beam Melting (EBM)," *Additive Manufacturing,* vol. 10, pp. 47-57, 2016.

[7] N. Hrabe and T. Quinn, "Effects of Processing on Microstructure and Mechanical Properties of A Titanium Alloy (Ti–6Al–4V) Fabricated Using Electron Beam Melting (EBM), Part 1: Distance from Build Plate and Part Size," *Materials Science and Engineering: A,* vol. 573, pp. 264-270, 2013.

[8] N. Hrabe and T. Quinn, "Effects of processing on microstructure and mechanical properties of a titanium alloy (Ti–6Al–4V) fabricated using electron beam melting (EBM), Part 2: Energy input, orientation, and location," *Materials Science and Engineering: A,* vol. 573, pp. 271-277, 6/20/ 2013.

[9] F. Luca, M. Emanuele, R. Pierfrancesco, and M. Alberto, "Microstructure and Mechanical Properties of Ti‐6Al‐4V Produced by Electron Beam Melting of Pre‐Alloyed Powders," *Rapid Prototyping Journal,* vol. 15, pp. 171-178, 2009.

[10] Q. Liu, Y. Wang, H. Zheng, K. Tang, L. Ding, H. Li*, et al.*, "Microstructure and mechanical properties of LMD–SLM hybrid forming Ti6Al4V alloy," *Materials Science and Engineering: A,* vol. 660, pp. 24-33, 4/13/ 2016.

[11] N. Moelans, B. Blanpain, and P. Wollants, "Quantitative Analysis of Grain Boundary Properties in A Generalized Phase Field Model For Grain Growth in Anisotropic Systems," *Physical Review B,* vol. 78, p. 024113, 2008.

[12] L. Wu, Y. Zhang, Y.-G. Jung, and J. Zhang, "Three-dimensional phase field based finite element study on Li intercalation-induced stress in polycrystalline LiCoO2," *Journal of Power Sources,* vol. 299, pp. 57-65, 12/20/ 2015.

[13] N. Moelans, B. Blanpain, and P. Wollants, "An Introduction to Phase-Field Modeling of Microstructure Evolution," *Calphad,* vol. 32, pp. 268-294, 2008.

[14] A. F. Ferreira, A. J. d. Silva, and J. A. d. Castro, "Simulation of The Solidification of Pure Nickel via The Phase-Field Method," *Materials Research,* vol. 9, pp. 349-356, 2006.

[15] R. Kobayashi, "Phase Field Simulations of Dendritic Solidification," in *Advanced Materials* ed, 1994, pp. 529-532.

[16] S. G. Kim, W. T. Kim, and T. Suzuki, "Phase-Field Model for Binary Alloys," *Physical Review E,* vol. 60, pp. 7186-7197, 1999.
[17] Z. Bi and R. F. Sekerka, "Phase-Field Model of Solidification of A Binary Alloy," *Physica A: Statistical Mechanics and its Applications,* vol. 261, pp. 95-106, 1998.
[18] B. Echebarria, R. Folch, A. Karma, and M. Plapp, "Quantitative Phase-Field Model of Alloy Solidification," *Physical Review E,* vol. 70, p. 061604, 2004.
[19] J. C. Ramirez, C. Beckermann, A. Karma, and H. J. Diepers, "Phase-Field Modeling of Binary Alloy Solidification with Coupled Heat and Solute Diffusion," *Physical Review E,* vol. 69, p. 051607, 2004.
[20] X. Gong and K. Chou, "Phase-Field Modeling of Microstructure Evolution in Electron Beam Additive Manufacturing," *JOM,* vol. 67, pp. 1176-1182, 2015.
[21] S. Sahoo and K. Chou, "Phase-Field Simulation of Microstructure Evolution of Ti–6Al–4V in Electron Beam Additive Manufacturing Process," *Additive Manufacturing,* vol. 9, pp. 14-24, 2016.
[22] G. Supriyo, M. Li, O.-O. Nana, and E. G. Jonathan, "On the primary spacing and microsegregation of cellular dendrites in laser deposited Ni–Nb alloys," *Modelling and Simulation in Materials Science and Engineering,* vol. 25, p. 065002, 2017.
[23] L. Wu and J. Zhang, "Phase Field Simulation of Dendritic Solidification of Ti-6Al-4V During Additive Manufacturing Process," *JOM,* vol. 70, pp. 2392-2399, October 01 2018.
[24] L. Nastac, J. Valencia, J.Xu, and H. Dong, "Assessment of Solidification-Kinetics Parameters for Titanium-Base Alloys," *Proceedings of the International Symposium on Liquid Metals Processing and Casting,* pp. 207-233, 1999.
[25] L. Nastac, "Solute Redistribution, Liquid/Solid Interface Instability, and Initial Transient Regions during the Unidirectional Solidification of Ti-6-4 and Ti-17 Alloys," in *CFD Modeling and Simulation in Materials Processing*, ed: John Wiley & Sons, Inc., 2012, pp. 123-130.
[26] G. Supriyo, M. Li, O.-O. Nana, and E. G. Jonathan, "On The Primary Spacing and Microsegregation ff Cellular Dendrites in Laser Deposited Ni–Nb Alloys," *Modelling and Simulation in Materials Science and Engineering,* vol. 25, p. 065002, 2017.
[27] V. Fallah, M. Amoorezaei, N. Provatas, S. F. Corbin, and A. Khajepour, "Phase-Field Simulation of Solidification Morphology in Laser Powder Deposition of Ti–Nb Alloys," *Acta Materialia,* vol. 60, pp. 1633-1646, 2012.
[28] H. K. Rafi, N. V. Karthik, H. Gong, T. L. Starr, and B. E. Stucker, "Microstructures and Mechanical Properties of Ti6Al4V Parts Fabricated by Selective Laser Melting and Electron Beam Melting," *Journal of Materials Engineering and Performance,* vol. 22, pp. 3872-3883, 2013.
[29] T. F. Broderick, A. G. Jackson, H. Jones, and F. H. Froes, "The Effect of Cooling Conditions on The Microstructure of Rapidly Solidified Ti-6Al-4V," *Metallurgical Transactions A,* vol. 16, pp. 1951-1959, 1985.
[30] M. H. Burden and J. D. Hunt, "Cellular and Dendritic Growth. I," *Journal of Crystal Growth,* vol. 22, pp. 99-108, 1974.
[31] W. Kurz and D. J. Fisher, "Dendrite Growth at The Limit of Stability: Tip Radius and Spacing," *Acta Metallurgica,* vol. 29, pp. 11-20, 1981.